

# UNIT-DDPM: UNpaired Image Translation with Denoising Diffusion Probabilistic Models

Hiroshi Sasaki<sup>1</sup>, Chris G. Willcocks<sup>1</sup>, Toby P. Breckon<sup>1,2</sup>

Department of {<sup>1</sup>Computer Science | <sup>2</sup>Engineering}, Durham University, Durham, UK

## Abstract

We propose a novel unpaired image-to-image translation method that uses denoising diffusion probabilistic models without requiring adversarial training. Our method, UNpaired Image Translation with Denoising Diffusion Probabilistic Models (UNIT-DDPM), trains a generative model to infer the joint distribution of images over both domains as a Markov chain by minimising a denoising score matching objective conditioned on the other domain. In particular, we update both domain translation models simultaneously, and we generate target domain images by a denoising Markov Chain Monte Carlo approach that is conditioned on the input source domain images, based on Langevin dynamics. Our approach provides stable model training for image-to-image translation and generates high-quality image outputs. This enables state-of-the-art Fréchet Inception Distance (FID) performance on several public datasets, including both colour and multispectral imagery, significantly outperforming the contemporary adversarial image-to-image translation methods.

## 1. Introduction

Synthesising realistic images is a long-standing goal for computer vision as it enables beneficial and wide-ranging applications such as data augmentation in machine learning tasks, privacy protection, and cost reduction within data acquisition. While there are a wide variety of alternative approaches for image synthesis, such as physical simulation [7], fractal landscapes [31], and image editing [30], the use of stochastic generative modelling [46] continues to offer remarkable effectiveness in terms of fabricating similar but differing images in specific domains without any domain-specific knowledge. Notably, recent research on the generative modelling focuses on Deep Neural Networks (DNN) [10], namely deep generative models (DGNN) because of their potential modeling capability of real-world data modalities. Generative Adversarial Networks (GAN) [11], autoregressive models [12], flow-based models such as NICE [3],

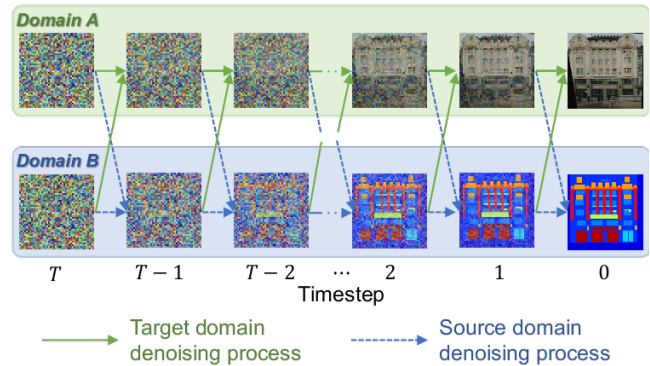


Figure 1: Conceptual illustration of our novel image-to-image translation approach using denoising diffusion probabilistic models.

RealNVP [4] and Glow [22], Variational Autoencoders (VAE) [32], and Image Transformer [29] have synthesized remarkably plausible images. Similarly, there have been significant advances in iterative generative models, such as Denoising Diffusion Probabilistic Models (DDPM) [15] and Noise Conditional Score Networks (NCSN) [38], which have demonstrated the ability to produce higher quality synthetic images comparable to that of other contemporary approaches, but without having to perform (potentially problematic) adversarial training. To achieve this, many denoising autoencoding models are trained to denoise samples corrupted by various levels of Gaussian noise. Samples are then produced via a Markov Chain Monte Carlo (MCMC) process, starting from white noise, which is progressively denoised and transformed into meaningful high-quality images. This generative Markov Chain process is based on Langevin dynamics [36] by reversing a forward diffusion process that progressively transforms images into noise.

DGNN has also attracted significant attention within image-to-image (I2I) translation [8] [20] [19] [44]. I2I translation is a computer vision task to model the mapping between different visual domains, such as style transfer [8],

Table 1: Fréchet Inception Distance (FID) [14] score on different image-to-image translation methods.

	Facades		Photos-Maps		Summer-Winter		RGB-Thermal	
	B→A	A→B	B→A	A→B	B→A	A→B	B→A	A→B
CycleGAN [44]	232.12	265.70	216.89	150.23	121.18	133.16	338.30	169.38
UNIT [25]	239.58	216.27	213.65	253.98	202.88	161.10	286.90	213.08
MUNIT [16]	335.72	244.78	240.11	224.96	221.11	205.33	305.24	233.92
DRIT++ [24]	336.76	317.23	316.42	237.94	261.82	268.45	284.21	226.35
UNIT-DDPM (Ours)	<b>169.95</b>	<b>110.13</b>	<b>193.06</b>	<b>116.23</b>	<b>113.70</b>	<b>109.98</b>	<b>198.85</b>	<b>167.70</b>

colourisation [5], super-resolution [23], photorealistic image synthesis [2], and domain adaptation [26]. For style transfer, a style transfer network [8] was proposed as the DNN that is trained to transfer the style from one image to another while preserving its semantic content. In addition, style transfer networks are used in the randomisation of image styles [20]. For general purposes, Pix2Pix [19] employs a GAN to model the mapping function using paired training data. To relax the dependency of the paired training, Cycle-consistent GAN (CycleGAN) [44] was proposed by leveraging cycle consistency to regularise the training. However, such GAN-based approaches require very specific choices in optimisation and architectures to stabilise training and can readily fail to cover all modes of the data distribution [9].

This paper proposes a new I2I translation approach that uses DDPM as its backend, instead of adversarial networks, in order to mitigate this limitation of unstable training and improve the quality of generated images (Figure 1). The main contributions of this paper are:

- *Dual-domain Markov Chain based Generative Model* – a Markov chain I2I translation approach is introduced that approximates the data distribution of both the source and target domains, such that they interrelate with each other (Section 3).
- *Stable Non-GAN-based Image-to-Image Translation Training* – the approach does not require adversarial training, however the model generates realistic outputs that capture high-frequency variations according to the perturbations of various levels of noise (Section 3.1).
- *Novel use of Markov Chain Monte Carlo Sampling* – the proposed sampling algorithm can be conditioned on unpaired source domain images to synthesise target domain images (Section 3.2).
- *State-Of-The-Art Image-to-Image Translation* – the results are found to outperform the prior work of CycleGAN [44], UNIT [25], MUNIT [16], and DRIT++ [24] qualitatively and quantitatively for a number of varied benchmark datasets (Facade [39],

Photos-Maps [44], Summer-Winter [44], and RGB-Thermal [17]) (Table 1 and Figure 5), as described in detail in Section 4.

## 2. Related Work

We review prior work in two relevant topics: image-to-image translation and denoising diffusion probabilistic models.

### 2.1. Image-to-Image Translation

The goal of I2I translation is learning a mapping between images from a source domain and images from a target domain, and I2I translation is generally classified into two types of approach: paired and unpaired.

#### 2.1.1 Paired Image-to-Image Translation

Supervised I2I approaches aim to learn the mapping between an input image and an output image using a training set of aligned image pairs. Earlier work proposed to use a pre-trained CNN and Gram matrices to obtain the perceptual decomposition of images [6]. This separates the image content and style, enabling style variation whilst preserving the semantic content. Many recent I2I approaches are trained adversarially with a GAN [11], which is a generative model designed to have a generator and a discriminator component that compete against each other. The generator is trained to map randomised values to real data examples by the discriminator output. The discriminator is simultaneously trained to discriminate real and fake data examples produced by the generator. Pix2Pix [19] provides a general-purposed adversarial framework to transform an image from one domain to another. Instead of an autoencoder, U-Net [34] is utilized to share the low-level information between the input and output. BicycleGAN [45] combines conditional VAE-GAN (CVAE-GAN) with an approach to recover the latent codes, which improves performance, where the CVAE-GAN reconstructs category specific images [1].

### 2.1.2 Unpaired Image-to-Image Translation

While paired I2I translation requires aligned image pairs of source and target domains, unpaired approaches learn source and target image sets which are completely independent without paired examples between the two domains. CycleGAN [44] is an unpaired I2I translation approach using a GAN. CycleGAN modifies the generator  $G$  and discriminator  $D$  to transfer from source images  $x_s \in X_s$  to target images  $x_t \in X_t$ . This learns not only a lateral transform  $G$ , but also bilateral transform paths  $G_t(x_s), G_s(x_t)$ . In addition, this adopts a new loss measure named a cycle-consistency loss  $L_{\text{cyc}}(G_s, G_t)$ :

$$\begin{aligned} \mathcal{L}_{\text{cyc}}(G_s, G_t) = & \mathbb{E}_{x_s \in X_s} [\|G_s(G_t(x_s)) - x_s\|_1] \\ & + \mathbb{E}_{x_t \in X_t} [\|G_t(G_s(x_t)) - x_t\|_1], \end{aligned} \quad (1)$$

which enforces consistency between real images from each domain and their generated counterparts.

Unsupervised Image-to-Image Translation Networks (UNIT) [25] further make a shared-latent space assumption in their method. To address the multimodal problem, Multimodal UNIT (MUNIT) [16] and Diverse Image-to-Image Translation via Disentangled Representations (DRIT++) [24] adopt a disentangled representation, which separates domain-specific attributes and shared content information within images, to further realise diverse I2I translation from unpaired image samples.

### 2.2. Denoising Diffusion Probabilistic Models

Denoising Diffusion Probabilistic Models (DDPM) [15] sequentially corrupt images with increasing noise, and learn to reverse the corruption as a generative model. In particular, the generative process is defined as the reverse of a Markovian diffusion process which, starting from white noise, progressively denoises the sample into an image.

DDPM models data as latent variable of the form  $p_\theta(\mathbf{x}_0) := \int p_\theta(\mathbf{x}_{0:T}) dx_{1:T}$ , where  $\mathbf{x}_0 \sim q(\mathbf{x}_0)$  are images,  $T$  is the length of the Markov chain, and  $\mathbf{x}_1, \dots, \mathbf{x}_T$  are latents of the same dimensionally as the images.  $p_\theta(\mathbf{x}_{0:T})$  is a Markov-chain with learnt Gaussian transitions (the reverse process) where:

$$p_\theta(\mathbf{x}_{0:T}) := p(\mathbf{x}_T) \prod_{t=1}^T p_\theta(\mathbf{x}_{t-1}|\mathbf{x}_t) \quad (2)$$

$$p_\theta(\mathbf{x}_{t-1}|\mathbf{x}_t) = \mathcal{N}(\mathbf{x}_{t-1}; \mu_\theta(\mathbf{x}_t, t), \Sigma_\theta(\mathbf{x}_t, t)) \quad (3)$$

$$p(\mathbf{x}_T) = \mathcal{N}(\mathbf{x}_T; \mathbf{0}, \mathbf{I}) \quad (4)$$

DDPM additionally approximates the posterior  $q(\mathbf{x}_{1:T}|\mathbf{x}_0)$  in the forward process. This Markov-chain gradually adds

progressive Gaussian noise to the images:

$$q(\mathbf{x}_{1:T}|\mathbf{x}_0) := \prod_{t=1}^T q(\mathbf{x}_t|\mathbf{x}_{t-1}) \quad (5)$$

$$q(\mathbf{x}_t|\mathbf{x}_{t-1}) = \mathcal{N}(\mathbf{x}_t; \sqrt{\alpha_t}\mathbf{x}_{t-1}, (1 - \alpha_t)\mathbf{I}), \quad (6)$$

where  $\alpha_t \in \{\alpha_1, \dots, \alpha_T\}$  are scheduled weights of the noise, therefore Equation (5) gradually adds Gaussian noise according to a variance schedule  $\alpha_t$ . Equation (6) is a linear interpolation function of noise and images, which admits sampling  $\mathbf{x}_t$  at an arbitrary timestep  $t$  as:

$$\mathbf{x}_t(\mathbf{x}_0, \epsilon) = \sqrt{\bar{\alpha}_t}\mathbf{x}_0 + \sqrt{1 - \bar{\alpha}_t}\epsilon, \quad (7)$$

where  $\bar{\alpha}_t := \prod_{s=1}^t \alpha_s$  and  $\epsilon \sim \mathcal{N}(\mathbf{0}, \mathbf{I})$ . To approximate  $p_\theta(\mathbf{x}_{t-1}|\mathbf{x}_t)$ , DDPM optimises the model parameter  $\theta$  via denoising score matching (DSM) [41]. The loss function is thus redefined as a simpler form as:

$$\mathcal{L}_{\text{simple}}(\theta) = \mathbb{E}_{t, \mathbf{x}_0, \epsilon} [\|\epsilon - \epsilon_\theta(\mathbf{x}_t(\mathbf{x}_0, \epsilon), t)\|^2], \quad (8)$$

where  $\epsilon_\theta$  is a non-linear function predicting the added noise  $\epsilon$  from  $\mathbf{x}_t$  and  $t$ . Using an approximated  $\epsilon_\theta$ ,  $\mu_\theta$  can be predicted as:

$$\mu_\theta(\mathbf{x}_t, t) = \frac{1}{\sqrt{\alpha}} \left( \mathbf{x}_t - \frac{1 - \alpha_t}{\sqrt{1 - \bar{\alpha}_t}} \epsilon_\theta(\mathbf{x}_t, t) \right). \quad (9)$$

$\Sigma_\theta$  in Equation (3) is set as  $\Sigma_\theta(\mathbf{x}_t, t) = (1 - \alpha_t)\mathbf{I}$ . This admits sampling  $\mathbf{x}_{t-1}$  from  $\mathbf{x}_t$ :

$$\mathbf{x}_{t-1} = \mu_\theta(\mathbf{x}_t, t) + \Sigma_\theta(\mathbf{x}_t, t)\epsilon, \quad (10)$$

which leads to being able to sample  $\mathbf{x}_0$ .

Our method applies the latent information approximated via DDPM to learn different domains of images and hence it connects between the latents of those domains. As a result, it allows gradual samples from noise, progressively denoised to images, within the target domain in such a way that is related to the input source domain images.

## 3. Methodology

Our aim is to develop I2I translation between different domains of images whose distributions are formed as the joint probability of Equation (2) respectively. The method needs to learn the parameters of the models from a given dataset of source and target domains via empirical risk minimisation and subsequently be able to infer the target domain images from the corresponding source domain images.

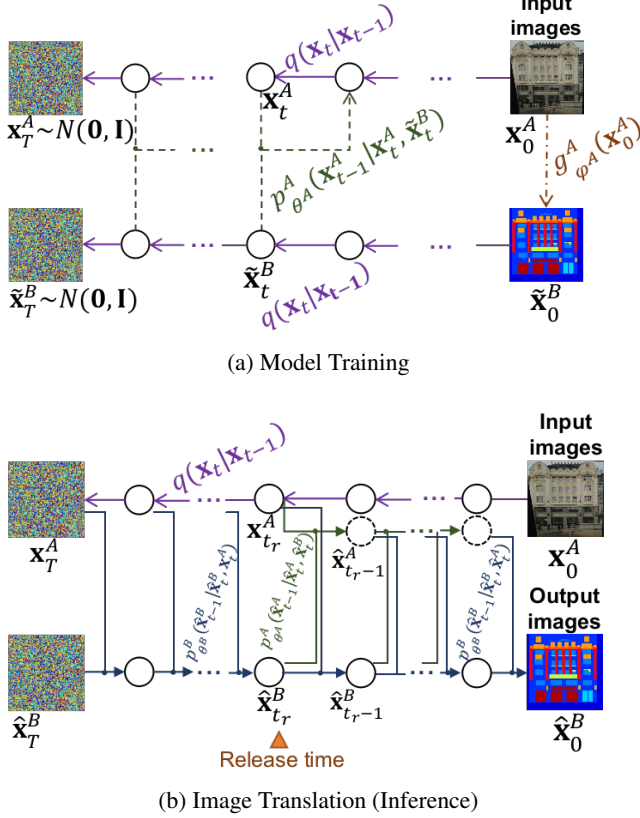


Figure 2: The processing flow of our method. Model training (top) and inference of image translation (inference) (bottom).

### 3.1. Model Training

Assuming a source domain  $\mathbf{x}_0^A \in \mathcal{X}^A$  and a target domain  $\mathbf{x}_0^B \in \mathcal{X}^B$ , we iteratively optimise the reverse process in each domain  $p_{\theta^A}^A, p_{\theta^B}^B$  and the domain translation functions  $\tilde{\mathbf{x}}_0^B = g_{\phi^A}^A(\mathbf{x}_0^A), \tilde{\mathbf{x}}_0^A = g_{\phi^B}^B(\mathbf{x}_0^B)$ , which are only used in the model training to transfer the domain A to B and B to A respectively, via DSM (Figure 2 (top)). To enable translation between source domain and target domain image pairs,  $p_{\theta^A}^A, p_{\theta^B}^B$  is modified as  $p_{\theta^A}^A(\mathbf{x}_{t-1}^A | \mathbf{x}_t^A, \tilde{\mathbf{x}}_t^B), p_{\theta^B}^B(\mathbf{x}_{t-1}^B | \mathbf{x}_t^B, \tilde{\mathbf{x}}_t^A)$  such as to be conditional on the generated images. On the reverse process optimisation step, the model parameters  $\theta^A, \theta^B$  are updated to minimise the loss function based on Equation (8), which is rewritten as:

$$\begin{aligned} \mathcal{L}_\theta(\theta^A, \theta^B) = & \mathbb{E}_{t, \mathbf{x}_0^A, \epsilon} [\|\epsilon - \epsilon_{\theta^A}^A(\mathbf{x}_t(\mathbf{x}_0^A, \epsilon), \tilde{\mathbf{x}}_t^B, t)\|^2] \\ & + \mathbb{E}_{t, \mathbf{x}_0^B, \epsilon} [\|\epsilon - \epsilon_{\theta^B}^B(\mathbf{x}_t(\mathbf{x}_0^B, \epsilon), \tilde{\mathbf{x}}_t^A, t)\|^2] \quad (11) \end{aligned}$$

The parameters of the domain translation functions  $\phi^A, \phi^B$  are updated to minimise the DSM objective fixing  $\theta^A, \theta^B$

### Algorithm 1 UNIT-DDPM Training

- 1: **repeat**
- 2:  $\mathbf{x}_0^A \in \mathcal{X}^A, \mathbf{x}_0^B \in \mathcal{X}^B$
- 3:  $\tilde{\mathbf{x}}_0^A \leftarrow g_{\phi^B}^B(\mathbf{x}_0^B), \tilde{\mathbf{x}}_0^B \leftarrow g_{\phi^A}^A(\mathbf{x}_0^A)$
- 4:  $t^A, t^B \sim \text{Uniform}(\{1, \dots, T\})$
- 5:  $\epsilon^A, \epsilon^B \sim \mathcal{N}(0, \mathbf{I})$
- 6:  $\mathbf{x}_{t^A}^A \leftarrow \sqrt{\bar{\alpha}_{t^A}} \mathbf{x}_0^A + \sqrt{1 - \bar{\alpha}_{t^A}} \epsilon^A$   
 $\mathbf{x}_{t^B}^B \leftarrow \sqrt{\bar{\alpha}_{t^B}} \mathbf{x}_0^B + \sqrt{1 - \bar{\alpha}_{t^B}} \epsilon^B$
- 7:  $\tilde{\mathbf{x}}_{t^A}^A \leftarrow \sqrt{\bar{\alpha}_{t^B}} \tilde{\mathbf{x}}_0^A + \sqrt{1 - \bar{\alpha}_{t^B}} \epsilon^A$   
 $\tilde{\mathbf{x}}_{t^B}^B \leftarrow \sqrt{\bar{\alpha}_{t^A}} \tilde{\mathbf{x}}_0^B + \sqrt{1 - \bar{\alpha}_{t^A}} \epsilon^B$
- 8: **Take gradient descent step on**  
 $\nabla_{\theta^A, \theta^B} [\|\epsilon^A - \epsilon_{\theta^A}^A(\mathbf{x}_{t^A}^A, \tilde{\mathbf{x}}_{t^A}^B, t^A)\|^2$   
 $\quad + \|\epsilon^B - \epsilon_{\theta^B}^B(\mathbf{x}_{t^B}^B, \tilde{\mathbf{x}}_{t^B}^A, t^B)\|^2]$
- 9: **Take gradient descent step on**  
 $\nabla_{\phi^A, \phi^B} [\|\epsilon^A - \epsilon_{\theta^A}^A(\mathbf{x}_{t^A}^A, \tilde{\mathbf{x}}_{t^A}^B, t^A)\|^2$   
 $\quad + \|\epsilon^A - \epsilon_{\theta^A}^A(\tilde{\mathbf{x}}_{t^B}^A, \mathbf{x}_{t^B}^B, t^B)\|^2$   
 $\quad + \|\epsilon^B - \epsilon_{\theta^B}^B(\mathbf{x}_{t^B}^B, \tilde{\mathbf{x}}_{t^B}^A, t^B)\|^2$   
 $\quad + \|\epsilon^B - \epsilon_{\theta^B}^B(\tilde{\mathbf{x}}_{t^A}^B, \mathbf{x}_{t^A}^A, t^A)\|^2$   
 $\quad + \lambda_{\text{cyc}} \|g_{\phi^B}^B(\tilde{\mathbf{x}}_0^B) - \mathbf{x}_0^A\|^2$   
 $\quad + \lambda_{\text{cyc}} \|g_{\phi^A}^A(\tilde{\mathbf{x}}_0^A) - \mathbf{x}_0^B\|^2]$
- 10: **until converged**

where:

$$\begin{aligned} \mathcal{L}_{\epsilon^\phi}(\phi^A, \phi^B) = & \mathbb{E}_{t, \mathbf{x}_0^B, \epsilon} [\|\epsilon - \epsilon_{\theta^A}^A(\mathbf{x}_t(g_{\phi^B}^B(\mathbf{x}_0^B), \epsilon), \mathbf{x}_t(\mathbf{x}_0^B, \epsilon), t)\|^2 \\ & + \|\epsilon - \epsilon_{\theta^B}^B(\mathbf{x}_t(\mathbf{x}_0^B, \epsilon), g_{\phi^B}^B(\mathbf{x}_t(\mathbf{x}_0^B, \epsilon), t))\|^2] \\ & + \mathbb{E}_{t, \mathbf{x}_0^A, \epsilon} [\|\epsilon - \epsilon_{\theta^B}^B(\mathbf{x}_t(g_{\phi^A}^A(\mathbf{x}_0^A), \epsilon), \mathbf{x}_t(\mathbf{x}_0^A, \epsilon), t)\|^2 \\ & + \|\epsilon - \epsilon_{\theta^A}^A(\mathbf{x}_t(\mathbf{x}_0^A, \epsilon), g_{\phi^A}^A(\mathbf{x}_t(\mathbf{x}_0^A, \epsilon), t))\|^2] \quad (12) \end{aligned}$$

In addition, the training is regularised by the cycle-consistency loss that is proposed in [44] to make both domain translation models bijective. The cycle-consistency loss, Equation (1) is rewritten as:

$$\begin{aligned} \mathcal{L}_{\text{cyc}^\phi}(\phi^A, \phi^B) = & \mathbb{E}_{\mathbf{x}_0^B} [\|g_{\phi^A}^A(g_{\phi^B}^B(\mathbf{x}_0^B)) - \mathbf{x}_0^B\|_1] \\ & + \mathbb{E}_{\mathbf{x}_0^A} [\|g_{\phi^B}^B(g_{\phi^A}^A(\mathbf{x}_0^A)) - \mathbf{x}_0^A\|_1] \quad (13) \end{aligned}$$

The loss function is thus described as follows:

$$\mathcal{L}_\phi(\phi^A, \phi^B) = \mathcal{L}_{\epsilon^\phi}(\phi^A, \phi^B) + \lambda_{\text{cyc}} \mathcal{L}_{\text{cyc}^\phi}(\phi^A, \phi^B), \quad (14)$$

where  $\lambda_{\text{cyc}}$  is a cycle-consistency loss weight. The overall training process is presented in Algorithm 1.

### 3.2. Inference of Image Translation

Using the trained  $\theta^A, \theta^B$ , the input images are translated from source to target domain. The domain translation functions are no longer used in inference. Instead, the target domain images are progressively synthesised from

---

**Algorithm 2** UNIT-DDPM Inference ( $\mathcal{X}^A \rightarrow \mathcal{X}^B$ )

---

```
1:  $\mathbf{x}_0^A \in \mathcal{X}^A, \hat{\mathbf{x}}_T^B \sim \mathcal{N}(0, \mathbf{I})$ 
2: for  $t = T, \dots, t_r + 1$  do
3:    $\epsilon^A, \epsilon^B \sim \mathcal{N}(0, \mathbf{I})$ 
4:    $\hat{\mathbf{x}}_t^A = \sqrt{\bar{\alpha}_t} \mathbf{x}_0^A + \sqrt{1 - \bar{\alpha}_t} \epsilon^A$ 
5:    $\hat{\mathbf{x}}_{t-1}^B = \frac{1}{\sqrt{1 - \alpha_t}} (\hat{\mathbf{x}}_t^B - \frac{1 - \alpha_t}{\sqrt{1 - \bar{\alpha}_t}} \epsilon_{\theta^B}(\hat{\mathbf{x}}_t^B, \hat{\mathbf{x}}_t^A, t)) + \sigma_t \epsilon^B$ 
6: end for
7: for  $t = t_r, \dots, 1$  do
8:    $\epsilon^A, \epsilon^B \sim \mathcal{N}(0, \mathbf{I})$  if  $t > 1$ , else  $\epsilon^A, \epsilon^B = 0$ 
9:    $\hat{\mathbf{x}}_{t-1}^A = \frac{1}{\sqrt{1 - \alpha_t}} (\hat{\mathbf{x}}_t^A - \frac{1 - \alpha_t}{\sqrt{1 - \bar{\alpha}_t}} \epsilon_{\theta^A}(\hat{\mathbf{x}}_t^A, \hat{\mathbf{x}}_t^B, t)) + \sigma_t \epsilon^A$ 
10:   $\hat{\mathbf{x}}_{t-1}^B = \frac{1}{\sqrt{1 - \alpha_t}} (\hat{\mathbf{x}}_t^B - \frac{1 - \alpha_t}{\sqrt{1 - \bar{\alpha}_t}} \epsilon_{\theta^B}(\hat{\mathbf{x}}_t^B, \hat{\mathbf{x}}_t^A, t)) + \sigma_t \epsilon^B$ 
11: end for
12: return  $\hat{\mathbf{x}}_0^B$ 
```

---

Gaussian noise and the noisy source domain images. During sampling, the generative process is conditioned on the input source domain images that are perturbed by the forward process from  $t = T$  until an arbitrary timestep  $t_r \in [1, T]$ . This is then re-generated by the reverse process from this timestep, which we denote as the *release time* (Figure 2 (bottom)). The case of transferring from domain A  $\mathbf{x}_0^A$  to domain B  $\hat{\mathbf{x}}_0^B$  is described as:

$$\hat{\mathbf{x}}_{t-1}^B = \mu_{\theta^B}(\hat{\mathbf{x}}_t^B, \hat{\mathbf{x}}_t^A, t) + \Sigma_{\theta^B}(\mathbf{x}_t, t) \epsilon^B \quad (15)$$

$$\hat{\mathbf{x}}_{t-1}^A = \begin{cases} \sqrt{\bar{\alpha}_t} \mathbf{x}_0^A + \sqrt{1 - \bar{\alpha}_t} \epsilon^A & (t > t_r) \\ \mu_{\theta^A}(\hat{\mathbf{x}}_t^A, \hat{\mathbf{x}}_t^B, t) + \Sigma_{\theta^A}(\mathbf{x}_t, t) \epsilon^B & (t \leq t_r) \end{cases} \quad (16)$$

$$\hat{\mathbf{x}}_T^B, \epsilon^A, \epsilon^B \sim \mathcal{N}(0, \mathbf{I}) \quad (17)$$

The overall translation (inference) process is presented in Algorithm 2.

## 4. Evaluation

Our method is evaluated against prior unpaired I2I translation methods [44] [25] [16] [24] on public datasets where ground truth input-output pairs are available [39] [44] [17].

### 4.1. Baselines

The inferred output imagery from our proposed method is compared with that of CycleGAN [44], UNIT [25], MUNIT [16], and DRIT++ [24] both quantitatively (Tables 1) and qualitatively (Figures 5).

### 4.2. Datasets

We prepare the following datasets for the experiment. Every dataset includes two domains (here abbreviated to domain A and B) of images and separated into training and test datasets. All images are resized  $64 \times 64$  pixels in advance.

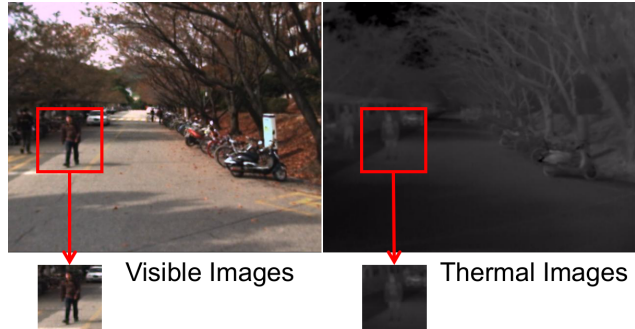


Figure 3: RGB-Thermal dataset cropped from the KAIST Multispectral Pedestrian Dataset[17].

**Facade** The (A) photo and (B) semantic segmentation label images of buildings from the CMP Facades dataset [39]. 400 pairs are included for training and 106 pairs for test.

**Photos-Maps** The (A) photo and (B) map images scraped from Google Maps [44]. 1,096 pairs are included for training and 1,098 pairs for test.

**Summer-Winter** The (A) summer and (B) winter Yosemite images downloaded using Flickr API [44]. The dataset includes 1,231 summer and 962 winter images for training and 309 summer and 238 winter images for test.

**RGB-Thermal** The (A) visible and (B) thermal infrared images of pedestrians from the KAIST Multispectral Pedestrian Dataset [17]. This dataset contains aligned visible and thermal images in various regular traffic scenes. Since the images are annotated the region of the pedestrians by bounding boxes, we crop 723 pairs of the pedestrian areas (more than  $64 \times 64$  pixels size) from the one scene (set00) for training and 425 pairs from another scene (set06) for test (Figure 3).

### 4.3. I2I translation via UNIT-DDPM

The denoising models of our method are implemented using U-Net [34] based on PixelCNN [35] and Wide ResNet [43], Transformer sinusoidal position embedding [40] to encode the timestep, whose length is  $T = 1000$ , and  $\alpha_t$  is linearly decreased from  $\alpha_1 = 0.9999$  to  $\alpha_T = 0.98$ , as same as original DDPM [15] but replaced Swish [33] with ReLU [27], group normalization [42] with batch normalization [18], and removed self-attention block to reduce the computation (Figure 4). The domain translation functions have ResNet [13] architecture which has same layer depth of the U-net. In training, the pair of the training sample and the fake another domain sample

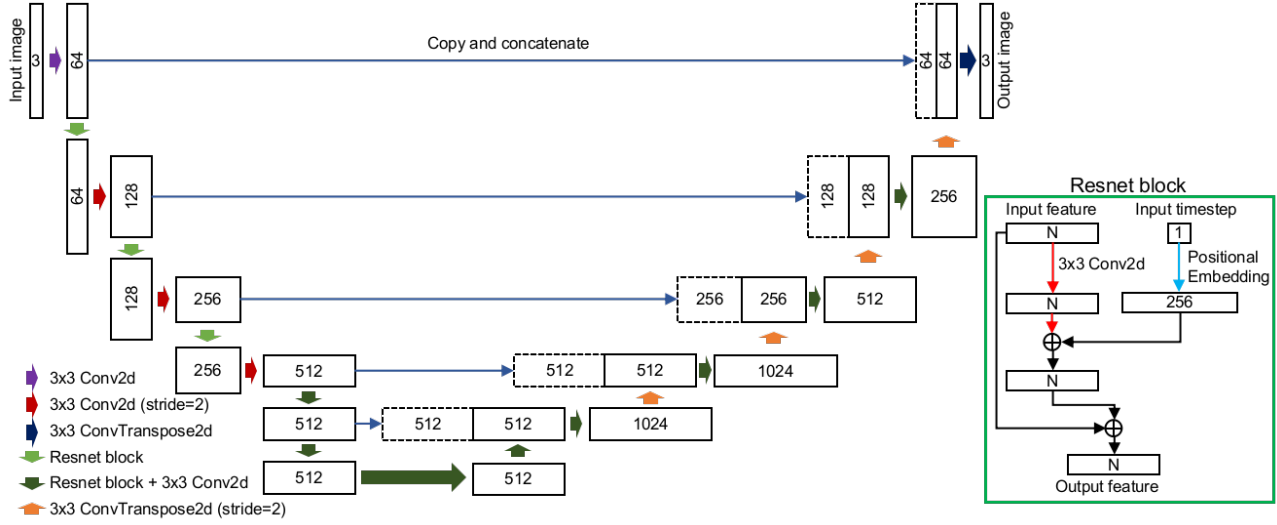


Figure 4: The diagram of our U-net architecture. Each Conv2d or ConvTranspose2d includes BatchNorm2d and ReLU before its input.

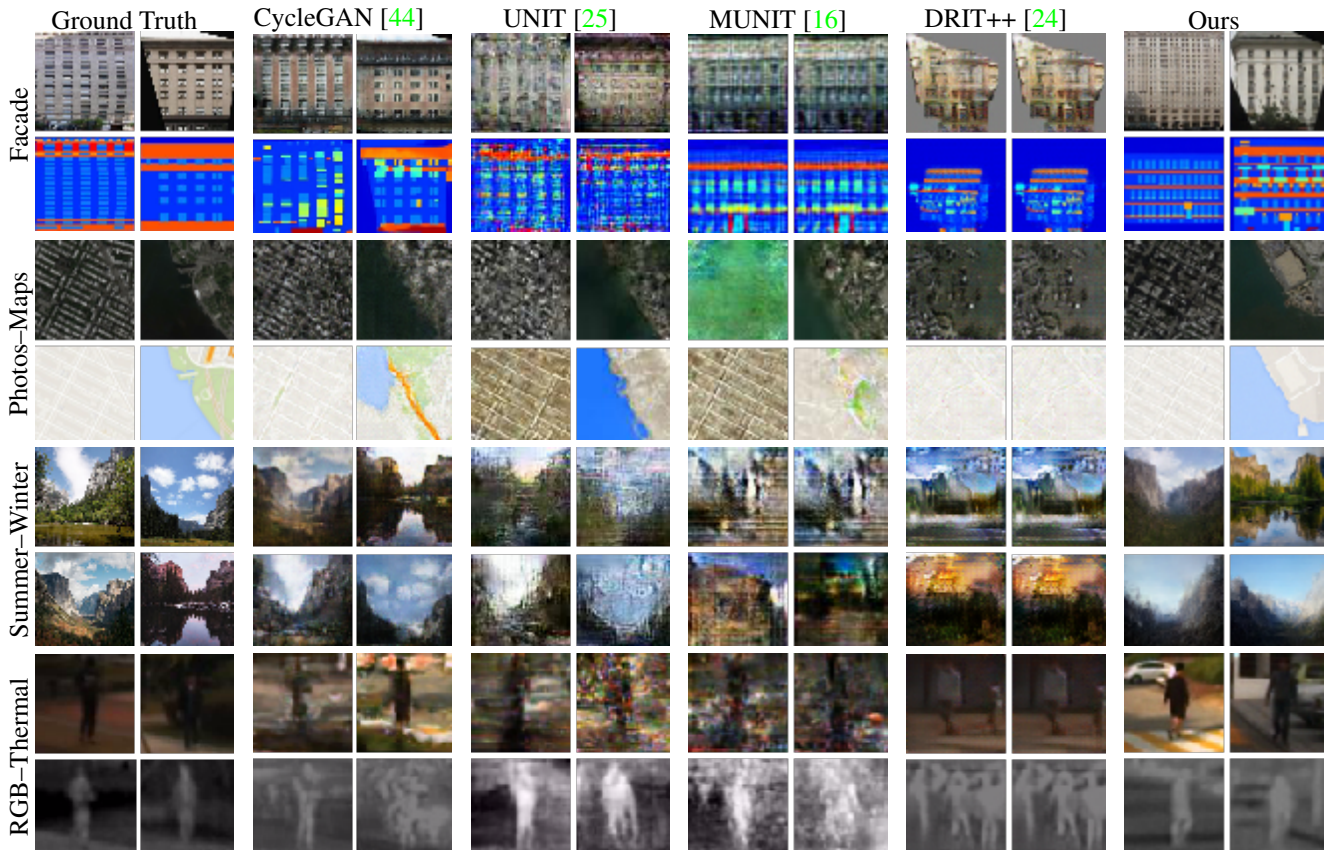


Figure 5: The examples of the output images generated by different image-to-image translation methods.

is concatenated as the input. The model parameters are updated with  $\lambda_{cyc} = 10.0$ , batch size  $B = 16$ , 20,000

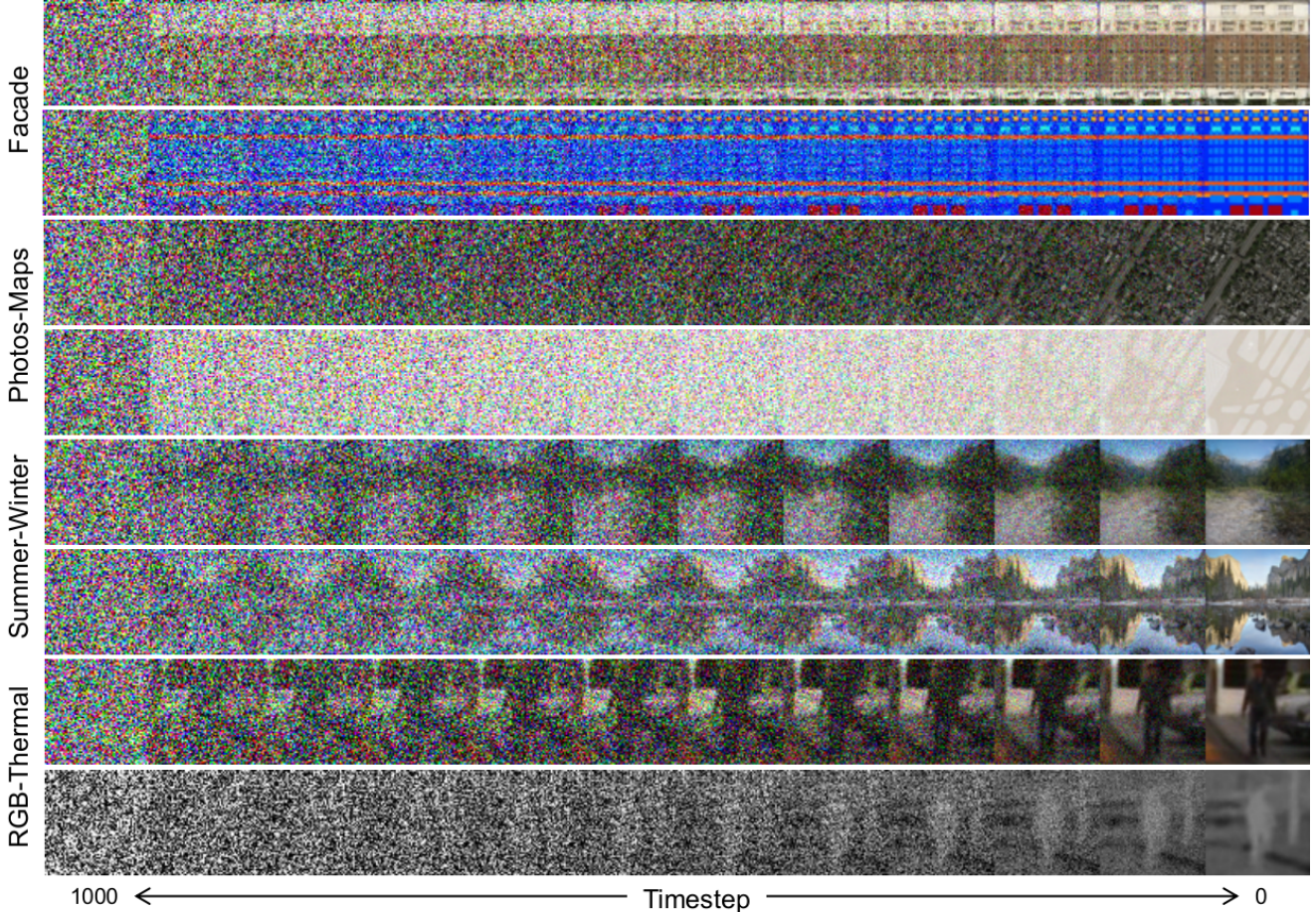


Figure 6: Examples of the progressive image generation via our method.

epochs via Adam [21] (initial learning rate  $\eta = 10^{-5}$ ,  $\beta_1 = 0.5$ ,  $\beta_2 = 0.999$ ).

We generate the images in both domains using the trained models and the test samples in each dataset with the *release time*  $t_r = 1$ .

#### 4.4. Result

The output images synthesised by each method are shown in Figure 5 from which it is clearly apparent that our approach qualitatively generates more realistic images than CycleGAN [44], UNIT [25], MUNIT [16], and DRIT++ [24]. We also found our method did not suffer from mode collapse at all and the resultant model training was more stable due to not requiring adversarial training. In addition, Figure 6 shows the progressive sampling via our method over the course of the reverse process. Comparison is conducted via Fréchet Inception Distance (FID) [14] between the ground truth and output images, and shown in Table 1. Our method outperforms the contemporary approaches of CycleGAN [44], UNIT [25],

MUNIT [16], and DRIT++ [24] over all of the benchmark datasets Facade, Photos-Maps, Summer-Winter, and RGB-Thermal offering a significant average increase in performance of  $\sim 20\%$  against previous approaches across all such datasets.

#### 4.5. Ablation Study

We analyse the impact of the *release time* against the performance by changing from  $t_r = 1$  to 900. The comparisons of the FID (Figure 7) show there are no significant change. We can observe slight differences attributable to the *release time* variation, but this is dataset dependent. This result suggests that the tuning of the *release time* hyperparameter is dataset dependent, from which further analysis represents a direction for future work.

#### 4.6. Limitations

We also observe the output images when the input image resolution is increased by  $256 \times 256$  pixels.

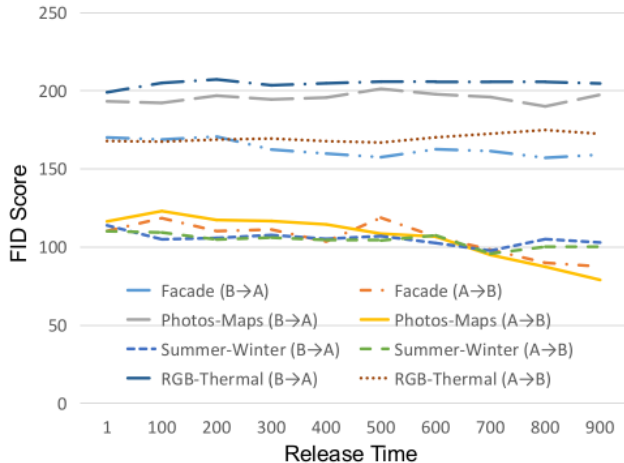


Figure 7: The comparison of FID by the release times.

The higher resolution models are trained using same network architecture (Figure 4) and learning parameters as Section. 4.3. The outputs shown in Figure 8 are wrongly coloured across the entire pixels. This suggests that the model fails to learn the global information of the images due to the increased complexity of the higher dimensional image space. One of the possible solution is adding more layers along with an attention mechanism into the U-net in the denoising models in order to capture much accurate multi-resolutional structure of images, which will be investigated in future work.

## 5. Conclusion

This paper proposes a novel unpaired I2I translation method that uses DDPM without adversarial training, named UNpaired Image Translation with Denoising Diffusion Probabilistic Models (UNIT-DDPM). Our method trains a generative model to infer the joint distribution of images over both domains as a Markov chain by minimising a DSM objective conditioned on the other domain. Subsequently, the domain translation models are simultaneously updated to minimise this DSM objective. After jointly optimising these generative and translation models, we generate target domain images by a denoising MCMC approach, which is conditioned on the input source domain images, based on Langevin dynamics. Our approach provides stable model training for I2I translation and generates high-quality image outputs. The experimental validation of our approach provides state-of-the-art FID score performance on several public datasets including both colour and multispectral imagery, significantly outperforming contemporary state of the art I2I translation methods.

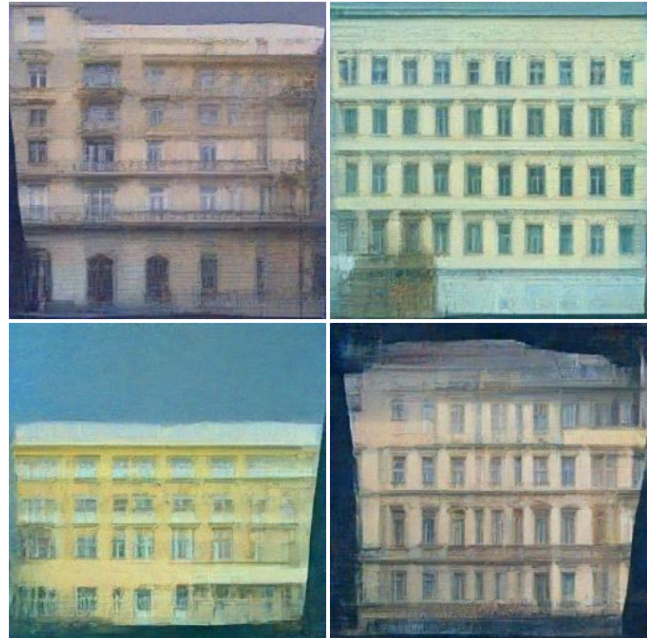


Figure 8: The examples of the output images of  $256 \times 256$  pixels generated using the model trained by our method (Facade dataset resized to  $256 \times 256$  pixels).

Although the experiment shows compelling results, the current form of our method is far from uniformly positive in particular in the case of larger resolution. To address this issue, the implementation needs to be modified to model large images much accurately.

In addition, one remaining drawback of DDPM is the inference time for image generation. However, this can be accelerated by modifying the Markovian process such as denoising diffusion implicit models [37] or reducing the timesteps using a learnable  $\Sigma_\theta$  [28].

Future work will consider modifications to enable shorter sampling times and higher quality image outputs, and the evaluation of the performance when the synthesised images are applied to other downstream computer vision tasks such as object classification.

## References

- [1] Jianmin Bao, Dong Chen, Fang Wen, Houqiang Li, and Gang Hua. Cvae-gan: fine-grained image generation through asymmetric training. In *Proc. of the IEEE Intl. Conf. on Computer Vision*, 2017. 2
- [2] Qifeng Chen and Vladlen Koltun. Photographic image synthesis with cascaded refinement networks. In *Proc. of the IEEE Intl. Conf. on Computer Vision*, 2017. 2
- [3] Laurent Dinh, David Krueger, and Yoshua Bengio. Nice: Non-linear independent components estimation. *Proc. 3rd Intl Conf. on Learning Representations*, 2015. 1

- [4] Laurent Dinh, Jascha Sohl-Dickstein, and Samy Bengio. Density estimation using real nvp. In *Proc. 5th Intl Conf. on Learning Representations*, 2017. 1
- [5] Z. Dong, S. Kamata, and T.P. Breckon. Infrared image colorization using s-shape network. In *Proc. Intl. Conf. on Image Processing*, 2018. 2
- [6] Leon A. Gatys, Alexander S. Ecker, and Matthias Bethge. A neural algorithm of artistic style. *CoRR abs/1508.06576*, 2015. 2
- [7] G Gerhart, G Martin, and T Gonda. Thermal image modeling. In *Infrared Sensors and Sensor Fusion*. International Society for Optics and Photonics, 1987. 1
- [8] Golnaz Ghiasi, Honglak Lee, Manjunath Kudlur, Vincent Dumoulin, and Jonathon Shlens. Exploring the structure of a real-time, arbitrary neural artistic stylization network. In *Proc. British Machine Vision Conf.*, 2017. 1, 2
- [9] Ian Goodfellow. Nips 2016 tutorial: Generative adversarial networks. *CoRR abs/1701.00160*, 2017. 2
- [10] Ian Goodfellow, Yoshua Bengio, and Aaron C. Courville. Deep learning. *Nature*, 521:436–444, 2015. 1
- [11] Ian Goodfellow, Jean Pouget-Abadie, Mehdi Mirza, Bing Xu, David Warde-Farley, Sherjil Ozair, Aaron Courville, and Yoshua Bengio. Generative adversarial nets. In *Advances in Neural Information Processing Systems 27*. 2014. 1, 2
- [12] Karol Gregor, Ivo Danihelka, Andriy Mnih, Charles Blundell, and Daan Wierstra. Deep autoregressive networks. In *Proc. Intl. Conf. on Machine Learning*, 2014. 1
- [13] Kaiming He, Xiangyu Zhang, Shaoqing Ren, and Jian Sun. Deep residual learning for image recognition. In *Proc. of the IEEE Conf. on Computer Vision and Pattern Recognition*, 2016. 5
- [14] Martin Heusel, Hubert Ramsauer, Thomas Unterthiner, Bernhard Nessler, and Sepp Hochreiter. Gans trained by a two time-scale update rule converge to a local nash equilibrium. In *Proc. Advances in Neural Information Processing Systems 30*. 2017. 2, 7
- [15] Jonathan Ho, Ajay Jain, and Pieter Abbeel. Denoising diffusion probabilistic models. *arXiv preprint arXiv:2006.11239*, 2020. 1, 3, 5
- [16] Xun Huang, Ming-Yu Liu, Serge Belongie, and Jan Kautz. Multimodal unsupervised image-to-image translation. In *Proc. of the European Conf. on Computer Vision*, 2018. 2, 3, 5, 6, 7
- [17] Soonmin Hwang, Jaesik Park, Namil Kim, Yukyung Choi, and In So Kweon. Multispectral pedestrian detection: Benchmark dataset and baselines. In *Proc. of IEEE Conf. on Computer Vision and Pattern Recognition*, 2015. 2, 5
- [18] Sergey Ioffe and Christian Szegedy. Batch normalization: Accelerating deep network training by reducing internal covariate shift. In *Proc. Intl. Conf. on Machine Learning*, 2015. 5
- [19] Phillip Isola, Jun-Yan Zhu, Tinghui Zhou, and Alexei A Efros. Image-to-image translation with conditional adversarial networks. In *Proc. of the IEEE Conf. on Computer Vision and Pattern Recognition*, 2017. 1, 2
- [20] Philip T. G. Jackson, Amir Atapour Abarghouei, Stephen Bonner, Toby P. Breckon, and Boguslaw Obara. Style augmentation: Data augmentation via style randomization. In *Proc. IEEE Conf. on Computer Vision and Pattern Recognition Workshops*, 2019. 1, 2
- [21] Diederik P. Kingma and Jimmy Ba. Adam: A method for stochastic optimization. In *Proc. 3rd Intl. Conf. on Learning Representations*, 2015. 7
- [22] Durk P Kingma and Prafulla Dhariwal. Glow: Generative flow with invertible 1x1 convolutions. In *Proc. Advances in Neural Information Processing Systems 31*, 2018. 1
- [23] Christian Ledig, Lucas Theis, Ferenc Huszár, Jose Caballero, Andrew Cunningham, Alejandro Acosta, Andrew Aitken, Alykhan Tejani, Johannes Totz, Zehan Wang, et al. Photo-realistic single image super-resolution using a generative adversarial network. In *Proc. of the IEEE Conf. on Computer Vision and Pattern Recognition*, 2017. 2
- [24] Hsin-Ying Lee, Hung-Yu Tseng, Jia-Bin Huang, Maneesh Singh, and Ming-Hsuan Yang. Diverse image-to-image translation via disentangled representations. In *Proc. of the European Conf. on Computer Vision*, 2018. 2, 3, 5, 6, 7
- [25] Ming-Yu Liu, Thomas Breuel, and Jan Kautz. Unsupervised image-to-image translation networks. In *Advances in Neural Information Processing Systems 30*. 2017. 2, 3, 5, 6, 7
- [26] Zak Murez, Soheil Kolouri, David Kriegman, Ravi Ramamoorthi, and Kyungnam Kim. Image to image translation for domain adaptation. In *Proc. of the IEEE Conf. on Computer Vision and Pattern Recognition*, 2018. 2
- [27] Vinod Nair and Geoffrey E Hinton. Rectified linear units improve restricted boltzmann machines. In *Proc. of the 27th Intl. Conf. on Machine Learning*, 2010. 5
- [28] Alex Nichol and Prafulla Dhariwal. Improved denoising diffusion probabilistic models. *arXiv preprint arXiv:2102.09672*, 2021. 8
- [29] Niki Parmar, Ashish Vaswani, Jakob Uszkoreit, Łukasz Kaiser, Noam Shazeer, Alexander Ku, and Dustin Tran. Image transformer. In *Proc. 6th Intl Conf. on Learning Representations*, 2018. 1
- [30] Patrick Pérez, Michel Gangnet, and Andrew Blake. Poisson image editing. In *ACM SIGGRAPH 2003 Papers*, 2003. 1
- [31] Przemyslaw Prusinkiewicz and Mark Hammel. A fractal model of mountains and rivers. In *Graphics Interface*, 1993. 1
- [32] Yunchen Pu, Zhe Gan, Ricardo Henao, Xin Yuan, Chunyuan Li, Andrew Stevens, and Lawrence Carin. Variational autoencoder for deep learning of images, labels and captions. In *Advances in Neural Information Processing Systems 29*. 2016. 1
- [33] Prajit Ramachandran, Barret Zoph, and Quoc V. Le. Searching for activation functions. *CoRR abs/1710.05941*, 2017. 5
- [34] Olaf Ronneberger, Philipp Fischer, and Thomas Brox. U-net: Convolutional networks for biomedical image segmentation. In *Intl. Conf. on Medical Image Computing and Computer-Assisted Intervention*, 2015. 2, 5
- [35] Tim Salimans, Andrej Karpathy, Xi Chen, and Diederik P. Kingma. Pixelcnn++: A pixelcnn implementation with discretized logistic mixture likelihood and other modifications. In *Proc. 5th Intl Conf. on Learning Representations*, 2017. 5

- [36] Jascha Sohl-Dickstein, Eric Weiss, Niru Maheswaranathan, and Surya Ganguli. Deep unsupervised learning using nonequilibrium thermodynamics. In *Proc. of Machine Learning Research* 37, 2015. 1
- [37] Jiaming Song, Chenlin Meng, and Stefano Ermon. Denoising diffusion implicit models. *arXiv preprint arXiv:2010.02502*, 2020. 8
- [38] Yang Song and Stefano Ermon. Generative modeling by estimating gradients of the data distribution. In *Proc. Advances in Neural Information Processing Systems* 32. 2019. 1
- [39] Radim Tyleček and Radim Šára. Spatial pattern templates for recognition of objects with regular structure. In *German Conference on Pattern Recognition*, 2013. 2, 5
- [40] Ashish Vaswani, Noam Shazeer, Niki Parmar, Jakob Uszkoreit, Llion Jones, Aidan N Gomez, Łukasz Kaiser, and Illia Polosukhin. Attention is all you need. In *Proc. Advances in Neural Information Processing Systems* 30, 2017. 5
- [41] Pascal Vincent. A connection between score matching and denoising autoencoders. *Neural computation*, 23(7):1661–1674, 2011. 3
- [42] Yuxin Wu and Kaiming He. Group normalization. In *Proc. of the European Conf. on Computer Vision*, 2018. 5
- [43] Sergey Zagoruyko and Nikos Komodakis. Wide residual networks. In *Proc. of the British Machine Vision Conference*, 2016. 5
- [44] Jun-Yan Zhu, Taesung Park, Phillip Isola, and Alexei A. Efros. Unpaired image-to-image translation using cycle-consistent adversarial networks. In *Proc. IEEE Intl. Conf. on Computer Vision*, 2017. 1, 2, 3, 4, 5, 6, 7
- [45] Jun-Yan Zhu, Richard Zhang, Deepak Pathak, Trevor Darrell, Alexei A Efros, Oliver Wang, and Eli Shechtman. Toward multimodal image-to-image translation. In *Proc. Advances in Neural Information Processing Systems* 30. 2017. 2
- [46] Song-Chun Zhu. Statistical modeling and conceptualization of visual patterns. *IEEE Transactions on Pattern Analysis and Machine Intelligence*, 25(6):691–712, 2003. 1